International Journal of Fatigue 176 (2023) 107896

Contents lists available at ScienceDirect

International Journal of Fatigue

journal homepage: www.elsevier.com/locate/ijfatigue

High-temperature fatigue behavior of TC17 titanium alloy and influence of surface oxidation

Gen Li [a], Yiyun Guo [a,b], Shao-Shi Rui [a], Chengqi Sun [a,b,*]

[a] State Key Laboratory of Nonlinear Mechanics, Institute of Mechanics, Chinese Academy of Sciences, Beijing 100190, China
[b] School of Engineering Science, University of Chinese Academy of Sciences, Beijing 100049, China

ARTICLE INFO

Keywords:
TC17 titanium alloy
Low and high cycle fatigue
Failure mechanism
High temperature
Surface oxidation

ABSTRACT

The fatigue of TC17 titanium alloy at high temperature could present fatigue failure mode or mixed failure mode with ductile cracks and local regions of fatigue cracks. For the former, the surface crack initiation tends to occur for low fatigue life, a competition between surface and internal crack initiation presents for medium fatigue life, and the internal crack initiation tends to occur for long fatigue life. The oxidation has a negative effect for the fatigue life under high stress amplitudes. For the latter, the fatigue life is generally low and the oxidation has no harmful influence on fatigue life.

1. Introduction

Metallic materials and components in aero-engines are usually subjected to cyclic loadings in a high-temperature environment and could experience complicated influence of high temperature and oxidation [1–8]. Compared to the situation at room temperature, the high temperature could reduce materials' resistance to fatigue crack growth and decrease the fatigue strength [4,5,9–13]. Moreover, oxidation of the material could cause surface oxide penetration and make the surface become harder and more brittle [4,5], which also influences the crack initiation mechanism.

Existing studies have investigated the high-temperature fatigue failure behaviors and the influence of oxidation on titanium alloys and Ni-based superalloys used in aero-engines in low cycle fatigue (LCF), high cycle fatigue (HCF) and very high cycle fatigue (VHCF) regimes [4,5,10,14–17]. For example, Hardt et al. [14] conducted LCF tests for titanium alloy IMI834 at temperatures up to 650 ℃. They found that the crack initiated from planar slip bands at lower temperatures and the fatigue life largely depended on the maximum stress, but a brittle oxygen-rich layer formed around the surface at temperatures above 600 ℃ and it significantly reduced the fatigue life. In HCF and VHCF regimes, Liu et al. [4,15] conducted ultrasonic frequency fatigue tests for TC17 titanium alloy at 400 ℃ under different stress ratios and reported that all the failed specimens at $R = -1$ showed surface crack initiation due to oxide shedding or oxide intrusion, however, the specimens tested at $R > 0$ could fail from internal crack initiation due to basal or prismatic slip in α grains. Moreover, a competition mechanism between surface and internal crack initiation for titanium alloys at 400 ℃ and 450 ℃ have been reported by Li and Sun [5] and Zhao et al. [17] for the tests at $R = -1$, respectively, and the specimens failed from internal crack initiation tended to have longer fatigue life than those failed from surface crack initiation. Stinville et al. [16] also found a similar competition mechanism for a polycrystalline Ni-based superalloy at 540 ℃ to 650 ℃. Nevertheless, Zhao et al. [10] conducted ultrasonic frequency fatigue tests for single-crystal Ni-based superalloy at temperatures from 760 ℃ to 1100 ℃ and found that the specimens failed from internal crack initiation at lower temperatures in VHCF regime, but all the specimens failed from surface crack initiation at 1100 ℃ due to the oxide penetration. According to these studies, the influence of temperature and oxidation are different, and the two factors are usually coupled to influence the fatigue performance and failure mechanism. Therefore, it is necessary to decouple the effects of temperature and oxidation in fatigue studies to understand their influence mechanism.

Some researchers [12,18–21] compared high-temperature fatigue performance in vacuum and air to investigate the influence of oxidation on fatigue performance. Mendez et al. [12] compared LCF behavior of Ti6246 alloy in air and vacuum environments at different temperatures. The results indicated that the discrepancy of the fatigue life in air and vacuum was relatively small at room temperature, but at above 300 ℃, the fatigue behavior at high stress level in air was lower than that in vacuum due to dynamical interaction of oxygen and cyclic plastic deformation in air. Heckel and Christ [20] and Maier et al. [21]

* Corresponding author at: State Key Laboratory of Nonlinear Mechanics, Institute of Mechanics, Chinese Academy of Sciences, Beijing 100190, China.
E-mail addresses: ruishaoshi@imech.ac.cn (S.-S. Rui), scq@lnm.imech.ac.cn (C. Sun).

https://doi.org/10.1016/j.ijfatigue.2023.107896
Received 6 June 2023; Received in revised form 27 July 2023; Accepted 15 August 2023
Available online 16 August 2023

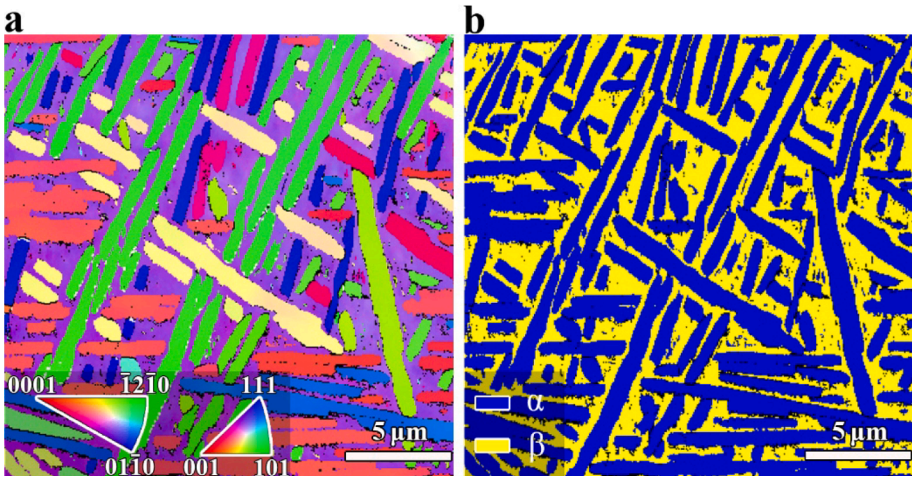

Fig. 1. Microstructure of the TC17 titanium alloy. (a) IPF, inset in (a) is color legend. (b) Phase map.

conducted high-temperature LCF tests for a titanium alloy and a titanium aluminide in air and vacuum, and found the negative effect of oxidation on the fatigue life. Although high-temperature fatigue tests in vacuum could make the specimens avoid oxidation, many tests were only in LCF regime due to the limitation of loading frequency. As another way to study the effect of oxidation, Cruchley et al. [22] applied prior oxidation on Ni-based superalloy specimens at 700 ℃ and compared the room-temperature HCF behavior of the pre-oxidized specimens and normal specimens, and found the negative effect of prior oxidation on the fatigue life in most scenarios, but they found that the prior oxidation could benefit the fatigue life in a limited stress range. Cervellon et al. [1] conducted ultrasonic frequency fatigue tests for single-crystal Ni-based superalloy at 1000 ℃ using normal and pre-oxidized specimens (1000 ℃ and 100 h). The specimens usually failed from internal pores in a life range of 10^7 to 10^9 cycles and the prior oxidation did not promote surface crack initiation. However, the specimens could fail from surface crack initiation due to oxidation in a longer life range of 10^9 to 10^{10} cycles. It is seen that the influence of oxidation is variable for different materials and temperatures. A clear understanding of this influence on material's fatigue performance in its working environment is important.

TC17 titanium alloy is usually used in compressor blades and blisks of aero-engines, which could experience oxidation at high temperature in service [5]. However, it is not clearly understood how oxidation in such a high-temperature environment affects the fatigue behavior and failure mechanism of this titanium alloy. The present paper aims to study the influence of oxidation at 400 ℃ on the fatigue behavior and failure mechanism of the TC17 titanium alloy. The fatigue specimens were prepared in three conditions, i.e., the initial specimens kept the initial state, the specimens pre-heated at 400 ℃ in air and experienced oxidation, and the specimens pre-heated at 400 ℃ in vacuum-like environment provided a control group that was heated but not oxidized. The fatigue tests at room and high temperatures were conducted, and the fatigue fracture morphology of the failed specimens was observed by scanning electron microscope (SEM). The oxygen distribution characteristics around the surface of the specimens were analyzed by energy dispersive spectroscopy (EDS), and the corresponding surface hardness was measured by a microhardness tester. The fatigue damage of specimens was also studied via SEM and electron backscatter diffraction (EBSD) observation.

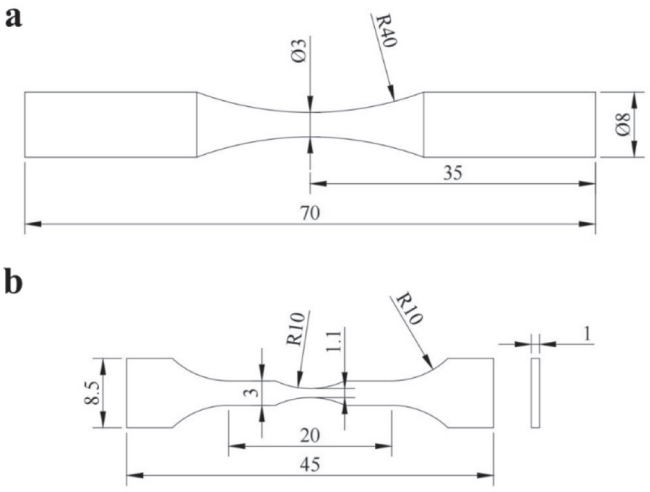

Fig. 2. Geometry of fatigue specimens (in mm). (a) The cylinder specimen used on MTS servo-hydraulic testing machine. (b) The plate specimen used on SEM in-situ fatigue test machine.

2. Experimental material and methods

2.1. Material

The TC17 titanium alloy with basketweave microstructure is used in this paper. The inverse pole figure (IPF) and phase map of the microstructure are shown in Fig. 1(a) and 1(b), respectively. The titanium alloy used in this study is the same as that in Refs. [5,23]. It consists of α and β phases, and the corresponding volume fractions are 0.692 and 0.276, respectively [5]. The chemical composition is given in Table 1. The heat treatment of the material started with solid solution at 800 ℃ for 4 h and was followed by water cooling. After that, the material was treated by thermal aging at 620 ℃ for 8 h and then was cooled in air. The yield strength and tensile strength of the TC17 titanium alloy at room temperature are 1047 MPa and 1141 MPa, respectively [5].

Table 1
Chemical composition of TC17 alloy.

Element	Al	Cr	Zr	Mo	Sn	O	Fe	H	C	Ti
Weight %	4.97	4.19	1.90	4.12	2.09	0.11	<0.10	0.0052	0.004	Balance

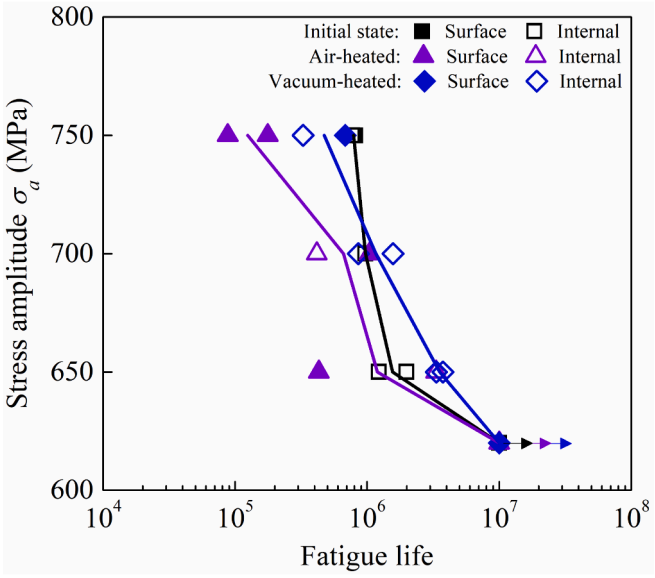

Fig. 3. S-N data at room temperature in air. The solid lines denote the mean fatigue life in logarithm of base 10, and the arrows denote the run-out specimens.

2.2. Fatigue tests and fractography

Two kinds of specimens are used for fatigue tests. One is the cylinder specimen in Fig. 2(a), and the other is the plate specimen in Fig. 2(b). Three conditions of the specimens are considered to decouple the influence of oxidation and temperature in high-temperature fatigue tests, i.e., the initial specimens, the specimens pre-heated at 400 ℃ for 2 h in air (named the air-heated specimens), and the specimens pre-heated at 400 ℃ for 2 h in vacuum-like environment (named the vacuum-heated specimens). The treatment of the vacuum-heated specimens started with placing the specimens in quartz tubes and the tubes were vacuumed by an air extractor and sealed, and then the specimens were heated in a muffle furnace for 2 h and cooled in air. Before pre-heating, the hourglass parts of the cylinder specimens were polished carefully along the loading direction to remove the machining scratches, and the plate specimens were polished to a mirror finish for SEM observation.

The cylinder specimens were tested on an MTS servo-hydraulic testing machine at room temperature in air, which was mainly used to investigate the influence of oxidation on HCF behavior. The loading frequency was 50 Hz, and the stress ratio was −1. The plate specimens were tested on an SEM in-situ fatigue test machine (Shimadzu SS-550) at 400 ℃ in vacuum-like environment (a vacuum degree of about 10^{-3} Pa), which was mainly used to investigate the influence of oxidation on LCF behavior. The loading frequency and the stress ratio are 10 Hz and 0.05, respectively.

After the fatigue tests, the fracture surfaces of failed specimens were observed by an SEM to identify the failure morphologies. The distribution of oxygen around the surface was analyzed by EDS. Some failed specimens were cut along the loading direction to investigate the damage behavior of the material, and these sections were polished to a mirror finish and characterized by EBSD. The surface hardness of the specimens in the three conditions was measured by a microhardness tester with a load of 50 gf and a holding time of 15 s to study the surface characteristics after oxidation.

3. Results

3.1. Fatigue tests at room temperature in air

Fig. 3 shows S-N data and the mean fatigue life in logarithm of base 10 for the specimens tested at room temperature in air. Table 2 provides the detailed results of these specimens. It is seen that the fatigue lives of the initial specimens and the vacuum-heated specimens are close for the stress amplitudes of 750 MPa, 700 MPa and 650 MPa. However, the fatigue life data of the air-heated specimens under 750 MPa are obviously lower than the other two groups, and the difference in fatigue lives between the air-heated specimens and the other two groups seems to be reduced under 700 MPa and 650 MPa. All the specimens in the three groups do not fail at 1×10^7 cycles under 620 MPa. These results indicate that the heating in air before fatigue tests could promote early failure under high stress amplitudes, but this trend is weaker with the decrease of the stress amplitude.

Table 2
Experimental results of specimens tested at room temperature in air ($R = -1$).

State of specimen	Specimen No.	σ_a (MPa)	N_f (cycles)	Crack initiation site
Initial specimens	1	750	7.7×10^5	Internal
	2	750	8.1×10^5	Surface
	3	700	9.7×10^5	Internal
	4	650	2.0×10^6	Internal
	5	650	1.2×10^6	Internal
	6	620	*1.0×10^7	–
Air-heated specimens	1	750	1.8×10^5	Surface
	2	750	8.8×10^4	Surface
	3	700	1.0×10^6	Surface
	4	700	4.2×10^5	Internal
	5	650	4.3×10^5	Surface
	6	650	3.3×10^6	Internal
	7	620	*1.0×10^7	–
Vacuum-heated specimens	1	750	3.3×10^5	Internal
	2	750	6.8×10^5	Surface
	3	700	8.6×10^5	Internal
	4	700	1.6×10^6	Internal
	5	650	3.3×10^6	Internal
	6	650	3.8×10^6	Internal
	7	620	*1.0×10^7	–

*It denotes that the specimen did not fail.

The fracture surfaces of all the failed specimens are observed by SEM. It is seen that the initial specimens and the vacuum-heated specimens mainly fail from internal crack initiation, and each of the two groups has one specimen showing surface crack initiation under the stress amplitude of 750 MPa. Fig. 4(a1-a3) and 4(c1-c3) show the fracture surface morphology of the internal crack initiation of the initial specimen and the vacuum-heated specimen, respectively. The surface crack initiation morphology of the initial specimen and the vacuum-heated specimen are shown in Fig. 4(b1-b3) and 4(d1-d3), respectively, and it could only happen for the specimens subjected to a high stress amplitude, such as 750 MPa. The air-heated specimens mainly fail from surface crack initiation, which is different from the other two groups. One air-heated specimen under 700 MPa fails from internal crack initiation as well as another air-heated specimen under 650 MPa fails from internal crack initiation. Fig. 4(e1-e3) and 4(f1-f3) show the fracture surface morphology of the internal crack initiation and surface crack initiation of the air-heated specimens, respectively. The fracture surface observation shows that the air-heated specimens tend to fail from surface crack initiation due to prior oxidation.

3.2. Fatigue tests at 400 ℃ in vacuum-like environment

Two stress amplitudes are determined for the in-situ fatigue tests at 400 ℃ in vacuum-like environment, viz 428 MPa and 418 MPa. Fig. 5 gives the S-N data for the specimens. Table 3 shows the detailed results of the specimens in Fig. 5. It shows that the fatigue life data of the three groups of specimens are quite close under the stress amplitude of 428 MPa, although the air-heated specimen has the highest fatigue life of 4.9

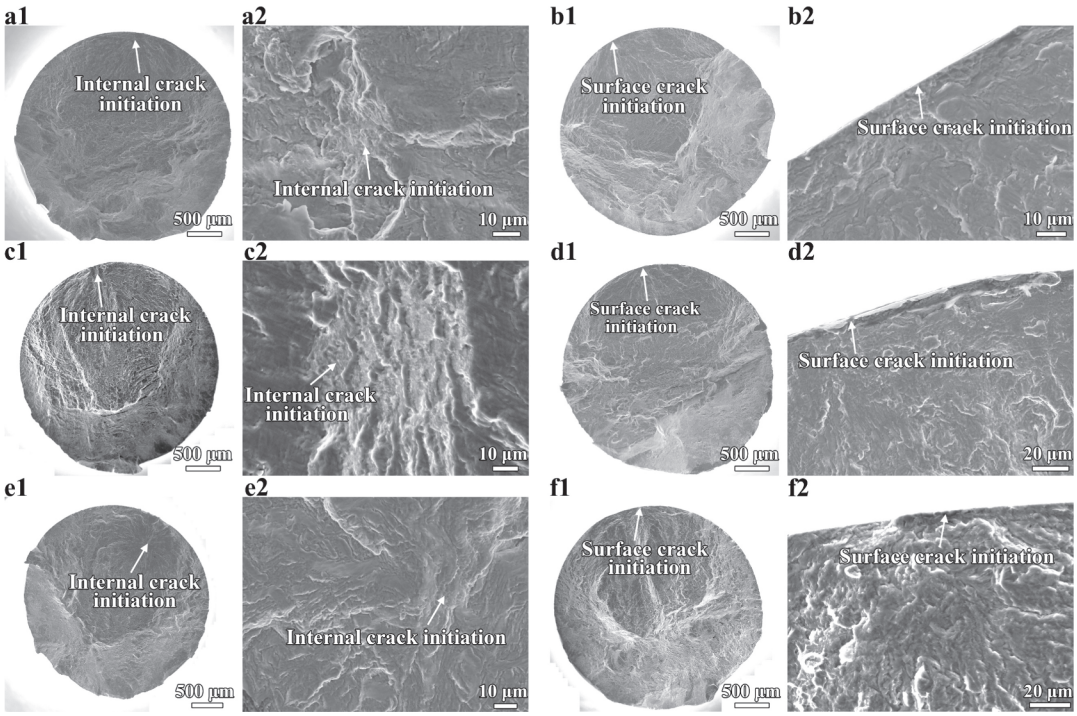

Fig. 4. Fracture surface of failed specimens tested at room temperature in air. (a1, a2) Initial specimen, σ_a=750 MPa and $N_f = 7.7 \times 10^5$ cycles, (a2) is enlarged view of the internal crack initiation region. (b1, b2) Initial specimen, σ_a=750 MPa and $N_f = 8.1 \times 10^5$ cycles, (b2) is enlarged view of the surface crack initiation region. (c1, c2) Vacuum-heated specimen, σ_a=700 MPa and $N_f = 8.6 \times 10^5$ cycles, (c2) is enlarged view of the internal crack initiation region. (d1, d2) Vacuum-heated specimen, σ_a=750 MPa and $N_f = 6.8 \times 10^5$ cycles, (d2) is enlarged view of the surface crack initiation region. (e1, e2) Air-heated specimen, σ_a=700 MPa and $N_f = 1.0 \times 10^6$ cycles, (e2) is enlarged view of the internal crack initiation region. (f1, f2) Air-heated specimen, σ_a=700 MPa and $N_f = 4.2 \times 10^5$ cycles, (f2) is enlarged view of the surface crack initiation region.

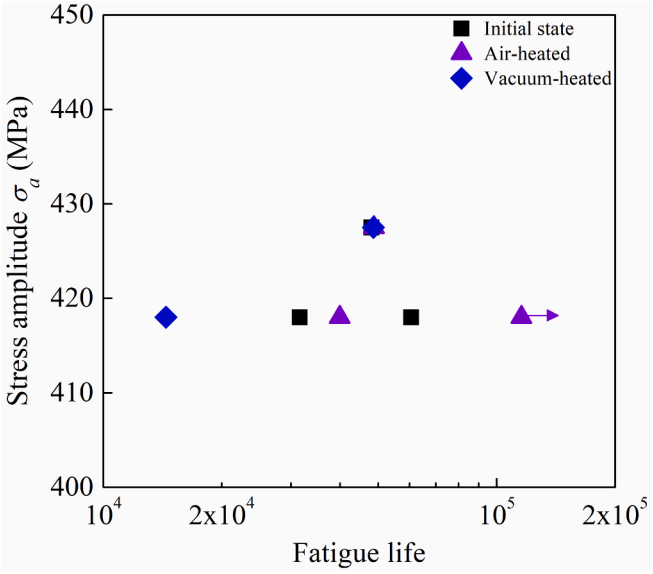

Fig. 5. S-N data tested at 400 ℃ in vacuum-like environment. The arrow denotes the run-out specimen.

$\times 10^4$ cycles among them. The initial specimens and the vacuum-heated specimens fail with fatigue lives in a range of 1.4×10^4 cycles to 6.1×10^4 cycles under the stress amplitude of 418 MPa. However, the air-heated specimens tend to have longer fatigue life under this stress amplitude, and one specimen does not fail exceeding 1×10^5 cycles, which is different from the result in Fig. 3.

Fig. 6 shows fracture surfaces of the failed specimens tested at 400 ℃ in vacuum-like environment. As shown in Fig. 6(a1), 6(b1), 6(c1) and 6(d1), the fracture surfaces of the three groups of specimens contain ductile fracture surface with dimples and one or several areas containing fatigue crack initiation and growth. Fig. 6(a2) and 6(b2) show the fracture surface morphology of the fatigue crack initiation from surface and interior for the initial specimens, respectively. Fig. 6(c2) shows the fracture surface morphology of the fatigue crack initiation from surface edge for the vacuum-heated specimen. The fatigue crack initiation from surface edge is also found for the initial specimens. Fig. 6(d2) and 6(d3) show the fracture surface morphology of the fatigue crack initiation from the interior and surface edge for the air-heated specimen, respectively. Fig. 6 indicates that the specimens tested at 400 ℃ in vacuum-like environment exhibit the mixed failure mode [24]. In this failure mode, both the ductile crack induced by plastic deformation and the fatigue crack induced by slip or local stress concentration play important roles in the failure. This failure mode is different from the fatigue crack dominated failure mode in Fig. 4. The harmless effect of oxidation on the

Table 3
Experimental results of specimens tested at 400 ℃ in vacuum-like environment ($R = 0.05$).

State of specimen	Specimen No.	σ_a (MPa)	N_f (cycles)	Failure mode
Initial specimens	1	428	4.8×10^4	Mixed mode
	2	418	6.1×10^4	Mixed mode
	3	418	3.2×10^4	Mixed mode
Air-heated specimens	1	428	4.9×10^4	Mixed mode
	2	418	4.0×10^4	Mixed mode
	3	418	*1.1×10^5	–
Vacuum-heated specimens	1	428	4.9×10^4	Mixed mode
	2	418	1.4×10^4	Mixed mode

*It denotes that the specimen did not fail.

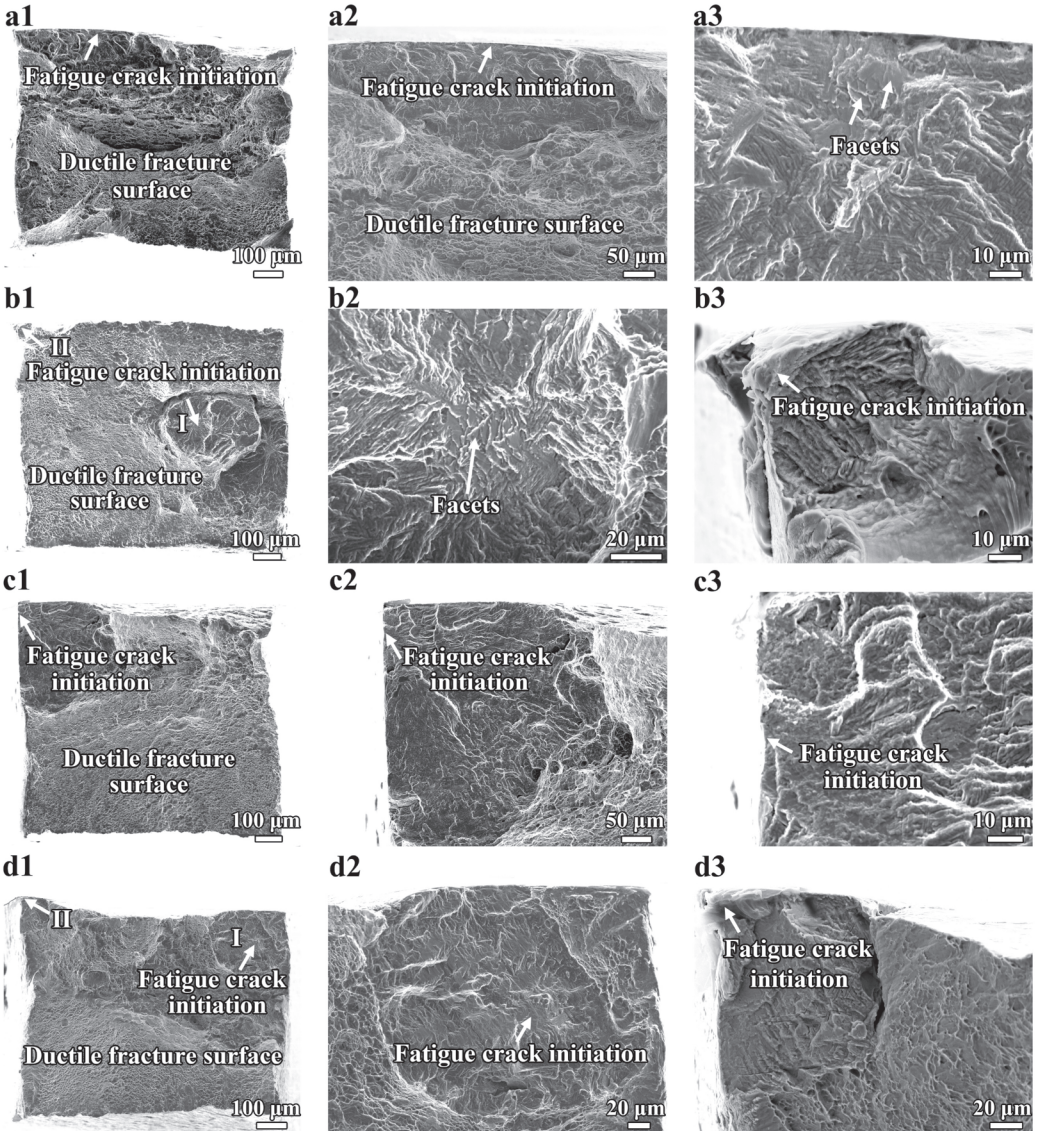

Fig. 6. Fracture surface of the failed specimens at 400 ℃. (a1-a3) Initial specimen, σ_a=418 MPa and N_f = 6.0 × 10^4 cycles, (a2) and (a3) are enlarged views of the crack initiation region. (b1-b3) Initial specimen, σ_a=428 MPa and N_f = 4.8 × 10^4 cycles, (b2) and (b3) are enlarged views of the crack initiation regions I and II in (b1), respectively. (c1-c3) Vacuum-heated specimen, σ_a=428 MPa and N_f = 4.9 × 10^4 cycles, (c2) and (c3) are enlarged views of the crack initiation region. (d1-d3) Air-heated specimen, σ_a=428 MPa and N_f = 4.9 × 10^4 cycles, (d2) and (d3) are enlarged views of the crack initiation regions I and II in (d1), respectively.

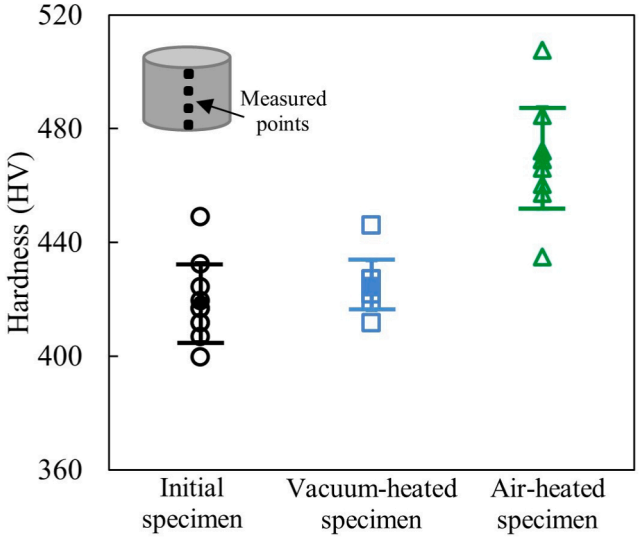

Fig. 7. Surface hardness of the cylinder specimens in three conditions.

S-N data in Fig. 5 could be attributed to that the oxidation inhibits the crack initiation at specimen surface, as discussed in Sec. 4.3.

4. Discussions

4.1. Influence of pre-heating in air and vacuum-like environment

The pre-heating at 400 ℃ in air causes oxidation around the surface of the specimens, and a clear understanding of the characteristics of oxidation is necessary to study its influence on the fatigue performance. The surface hardness of the cylinder specimens in three conditions is measured and shown in Fig. 7. The selected specimens for hardness tests were not used in the fatigue tests. Ten points were measured for each specimen, and the error bars in Fig. 7 presented the standard deviation of the hardness. The results indicate that the initial specimens and the vacuum-heated specimens have similar hardness, and the mean values are 419 HV and 425 HV, respectively. However, the air-heated specimens present higher hardness, and the mean value reaches 473 HV, which is 13.0% higher than that of the initial specimens. It shows that the pre-heating in vacuum-like environment does not significantly increase the surface hardness, and the improvement of surface hardness of the air-heated specimens is attributed to the oxidation at 400 °C in air. The oxide at surface is harder and more brittle than the substrate

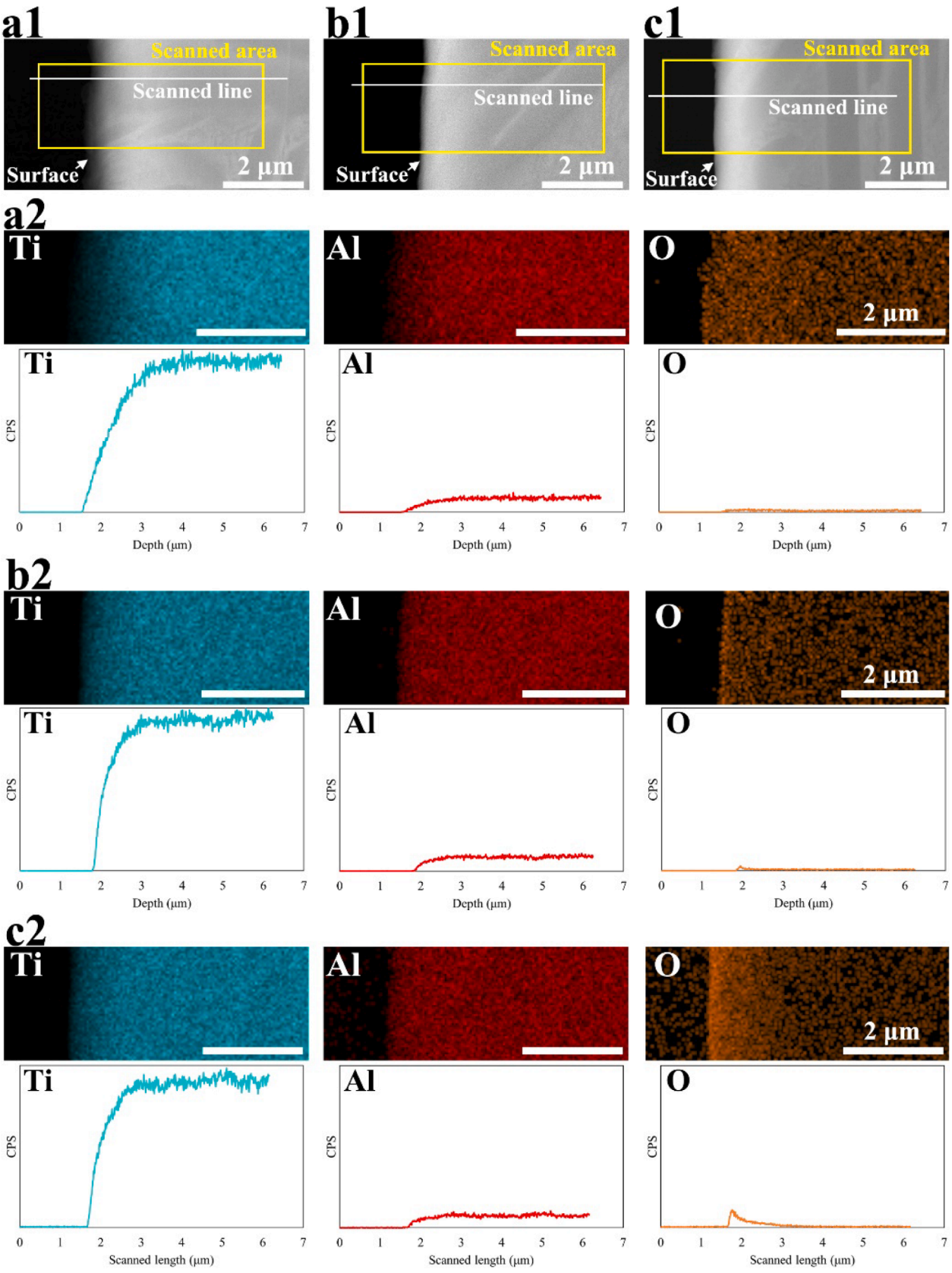

Fig. 8. Analysis of oxygen distribution from surface to interior by EDS. (a1), (b1) and (c1) are SEM images of a section on the initial specimen, vacuum-heated specimen and air-heated specimen, respectively. (a2), (b2) and (c2) are EDS maps of the scanned areas and lines in (a1), (b1) and (c1), respectively.

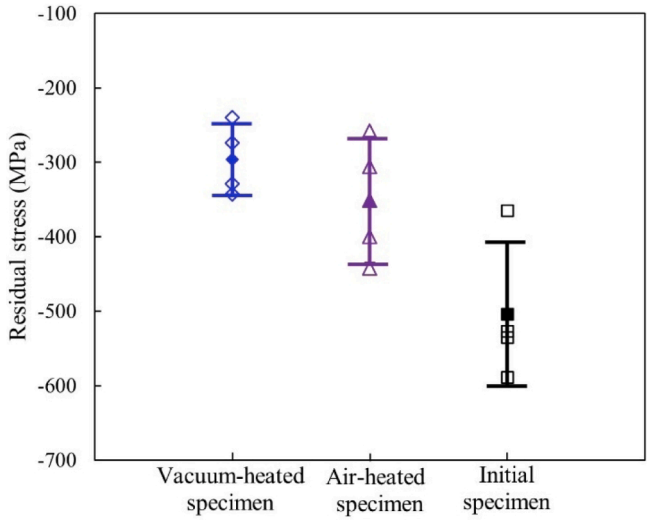

Fig. 9. Residual stress of the cylinder specimens along the loading direction.

material [25–27]. According to the results in Fig. 3 and the analysis in Ref. [5], the oxidized surface could induce surface crack initiation under high stress amplitudes.

The oxygen distribution around the surface was analyzed by EDS for the three groups of cylinder specimens. The EDS maps for the surface regions of the initial specimen, vacuum-heated specimen and air-heated specimen are shown in Fig. 8(a2), 8(b2) and 8(c2), respectively. The oxygen element in Fig. 8(a2) does not concentrate at the surface and is uniformly distributed in the map. It indicates that the initial specimen does not experience surface oxidation. The oxygen element in Fig. 8(b2) is slightly concentrated at the surface, indicating that the vacuum-heated specimen experiences minor surface oxidation. This is due to that the vacuum-heated specimens were put in the sealed quartz tubes during the heating process and the residual air in the tube caused minor surface oxidation. The oxygen distribution map and the scanned line in Fig. 8(c2) indicate that the oxygen element is concentrated at the surface for the air-heated specimens, and the surface oxygen-rich layer is quite thin, which is about 600 ~ 700 nm. Even though the surface oxygen-rich layer is such thin, the surface hardness of the air-heated specimen is higher than that of the other two groups of specimens in Fig. 7. According to Refs. [27–31], the surface oxygen-rich layer should include TiO_2 at the surface and oxygen diffusion zone below the surface oxide, which is harder than the substrate material.

Moreover, based on the results in Refs. [32–35], heating in vacuum-like environment is one of common methods to remove residual stress. The residual stress at the minimum section of the cylinder specimens in three conditions was measured by X-ray diffraction (XRD). Four measurement points with an interval of 90° were selected for each specimen. Fig. 9 shows the residual stress and error bars at the minimum section of the cylinder specimens. The direction of the residual stress was along the loading direction. It is seen that the initial cylinder specimens have high residual compressive stress with a mean value of −504 MPa and a standard deviation of 96.8 MPa, and the distribution of residual stress is nonuniform. After the vacuum-heating treatment, the residual compressive stress is reduced, and its distribution becomes more uniform. The mean value of residual stress is −296 MPa and the standard deviation is reduced to 48.0 MPa. While the mean value and standard deviation of the residual compressive stress of the air-heated specimen are higher than those of the vacuum-heated specimen, which might be due to that surface oxidation inhibits the relaxation of residual stress [36].

4.2. Fatigue failure mechanism at high temperature

The TC17 specimens tested at high temperature could fail from surface crack initiation or internal crack initiation [5]. To understand the influence of oxidation on the surface crack initiation, Fig. 10 compares the cylinder views of an initial specimen and an air-heated specimen failed from surface crack initiation, which are tested under the stress amplitude of 750 MPa at room temperature in air. Fig. 10(a) and 10(b) show that the cylinder around the fracture surface of the initial specimen mainly presents shear deformation, and there are no dense lateral cracks around the cylinder surface. However, the air-heated specimen in Fig. 10(c) and 10(d) shows dense lateral cracks, which are straight and short. Such crack feature is also reported for the pre-

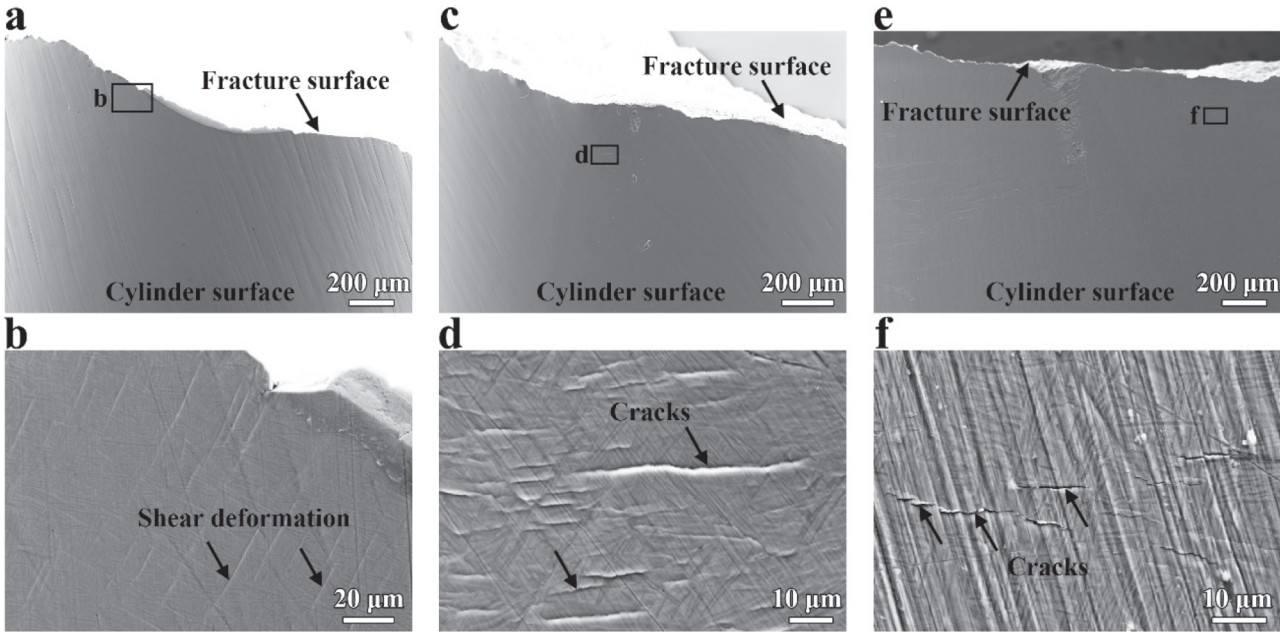

Fig. 10. Cylinder views of the failed specimens tested in air. (a) Initial specimen tested at room temperature in air, σ_a=750 MPa and $N_f = 8.1 \times 10^5$ cycles, (b) is the enlarged view of box b in (a). (c) Air-heated specimen tested at room temperature in air, σ_a=750 MPa and $N_f = 1.8 \times 10^5$ cycles, (d) is the enlarged view of box d in (c). (e) Specimen tested at 400 ℃ in air [5], σ_a=540 MPa and $N_f = 1.2 \times 10^5$ cycles, (f) is the enlarged views of box f in (e).

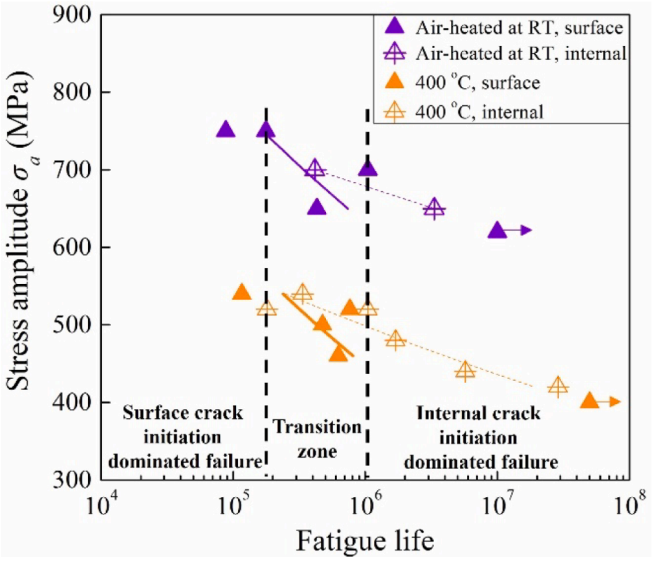

Fig. 11. S-N data of the air-heated specimens tested at room temperature (RT) in air and the TC17 specimens tested at 400 ℃ in air [5]. The arrows denote the run-out specimens.

oxidized specimens of Ni-based superalloy subjected to cyclic loadings in Refs. [1,10,22]. The dense lateral cracks should be due to that the hard and brittle oxygen-rich layer makes its deformation less compatible with that of the substrate material, and the high strain localization leads to the brittle fracture of oxygen-rich layer under high stress amplitudes. The cracking in oxygen-rich layer promotes the surface crack initiation of the oxidized specimen under high stress amplitudes and reduces the fatigue life, which supports that the air-heated specimens tend to fail from surface crack initiation in Fig. 3. The similar failure mechanism due to the surface brittle cracking of oxide coating was also reported for the coated aluminum alloys under cyclic loadings [37,38]. Moreover, the dense lateral cracks with straight and short features are found on the surface of the failed specimen of the same TC17 alloy tested at 400 ℃ in air [5], as shown in Fig. 10(e) and 10(f), which further confirms that the cracking feature is due to the fracture of oxygen-rich layer.

Apart from the surface crack initiation, those specimens tested at high temperature with longer fatigue life could fail from the internal crack initiation, and this failure mode has been discussed in Ref. [5]. The internal crack initiation at high temperature could be due to that the microstructure inhomogeneity causes strain localization under cyclic loadings, which aggravates the dislocation accumulation or grain refinement, and further promotes the internal crack nucleation and the failure of specimens.

Fig. 11 shows the S-N data of the air-heated specimens tested at room temperature and the specimens of the same TC17 titanium alloy tested at 400 ℃ in Ref. [5]. It is seen that both surface crack initiation and internal crack initiation could happen for the oxidized specimens tested at room temperature and high temperature in air, and the variation trends of the S-N data of the two groups are similar. According to the fatigue life in Fig. 11, the failure mode could be divided into three types, viz surface crack initiation dominated failure, transition zone and internal crack initiation dominated failure. The surface crack initiation is a common failure mode for titanium alloys at high temperatures in LCF regime [3,12,14,20,39–41], and the specimens experienced oxidation in air generally own lower fatigue life than those tested in vacuum [12,20,21]. Therefore, based on the analysis in Fig. 11 and LCF studies in literature [3,12,14,20,39–41], a variation of the fatigue crack initiation mode of the TC17 titanium alloy from LCF to VHCF regimes at high temperature in air could be summarized as follows. Under high stress amplitudes, the specimens mainly fail from surface crack initiation, and it could be induced by brittle fracture of oxidized surface, and oxidation presents the negative effect in this regime. With a decrease of stress amplitude, both surface and internal crack initiation could happen in the life range of transition zone. At this state, the negative effect of oxidation on the fatigue life decreases. Subsequently, at relative lower stress amplitudes, the specimens mainly fail from internal crack initiation due to microstructure inhomogeneity and damage accumulation. The crack initiation is irrespective of the influence of surface oxide in this situation.

4.3. Mechanism of mixed failure mode at high temperature

The plate specimens tested in vacuum-like environment at 400 ℃ and $R = 0.05$ present the mixed failure mode (i.e., the failure is due to the combination of plastic deformation and fatigue cracks), as shown in Fig. 6, and this failure mode is different from the typical fatigue failure induced by fatigue crack initiation and growth. To further understand the fatigue behavior of the specimens failed from the mixed failure mode and the influence of oxidation, the side views of the three kinds of specimens were observed by SEM, and the sectional views of the specimens were studied through EBSD characterization.

Fig. 12(a1-a3) and 12(b1-b3) show side views of the initial specimen and the vacuum-heated specimen tested at 400 ℃ in vacuum-like environment, respectively. Both specimens present a large area of lateral cracks and a local area of shear deformation and shear cracks around the fracture surface in Fig. 12(a1) and 12(b1). The lateral cracks are approximately perpendicular to the loading direction, and the shear deformation as well as the shear cracks are about 45° of the loading direction. When the sight moves to the area about 600 μm away from the fracture surface, as shown in Fig. 12(a3) and 12(b3), the lateral cracks are still a dominant feature in the side views of the two specimens. It indicates that the specimens' surface without oxidation presents the feature of many ductile cracks. The shear deformation is less significant in the two groups of specimens. However, the side view around the fracture surface of the air-heated specimen tested at 400 ℃ in vacuum-like environment presents a large area of shear deformation and a local region of lateral cracks, and the area about 600 μm away from the fracture surface generally presents shear deformation feature, as shown in Fig. 12(c1-c3). The difference between the air-heated specimen and the other two groups of specimens should be due to the harder oxidized surface restricting the initiation and development of ductile cracks at the surface to some extent. In this way, the oxidation at specimen surface improves the fatigue life, as observed for the air-heated specimens in Fig. 5.

Fig. 13(a1) shows the sectional view of an air-heated specimen tested at 400 ℃ in vacuum-like environment, which presents a deep hole in the specimen. Fig. 13(a2-a4) shows the magnified views of the deep hole and a range of crack propagation around the deep hole. Micro voids and dimple features are found in the deep hole, which indicates that the deep hole could be produced by plastic deformation and growth of ductile cracks at high temperature. To understand the formation of the voids, Fig. 13(b1-b5) shows two voids and the nearby microstructure in the section. The two voids are formed around the boundary of an α grain and β phase. According to the kernel average misorientation (KAM) image (Fig. 13(b3)), the α grain experiences significant deformation. The Schmid factor (SF) in Fig. 13(b4) and 13(b5) shows that the nearby α grains have high SF values on pyramidal plane. Similar voids have been reported for titanium alloys under fatigue loadings ($R \geq 0$) at room and high temperatures [42–44]. The voids were formed mainly due to dislocation pile-ups at the boundary of α/β phase, and then the pyramidal slip and basal slip impinging on the boundary and promoting the local fracture [43–45]. Fig. 13(c1)-(c3) presents SEM image, IPF and KAM of the region including the crack propagation in Fig. 13(a2), respectively. It is seen that this crack should be formed through coalescing voids under fatigue loadings. The SF in Fig. 13(c4) and 13(c5) shows that the nearby α grains have high SF values on basal plane and pyramidal plane, which supports that the pyramidal slip and basal slip favor accumulation of local plastic strain and promote the formation of

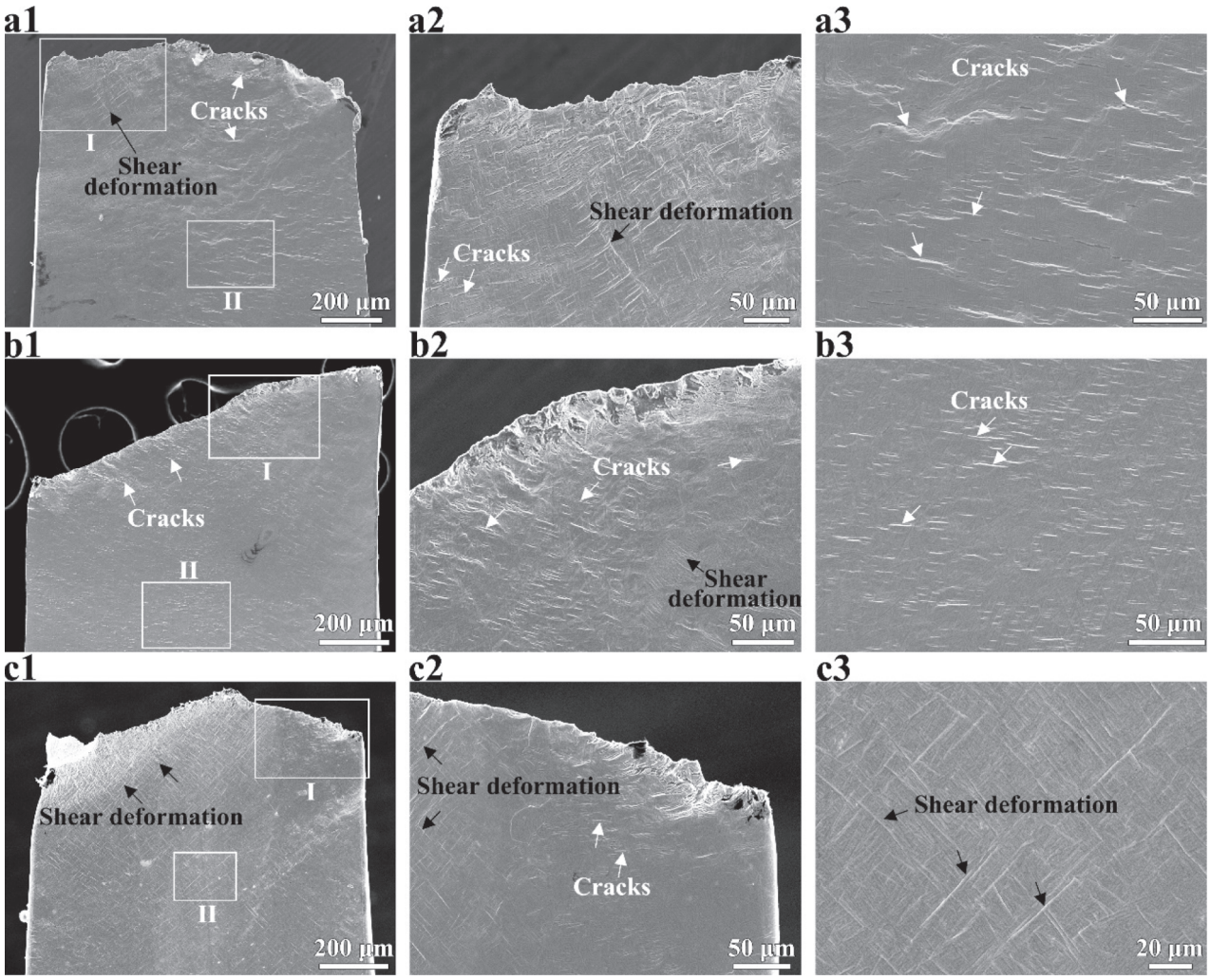

Fig. 12. Side views of failed specimens tested at 400 ℃ in vacuum-like environment. (a1-a3) Initial specimen with numerous lateral cracks, σ_a=428 MPa and $N_f = 4.8 \times 10^4$ cycles, (a2) and (a3) are enlarged views of boxes I and II in (a1), respectively. (b1-b3) Vacuum-heated specimen with numerous lateral cracks, σ_a=428 MPa and $N_f = 4.9 \times 10^4$ cycles, (b2) and (b3) are enlarged views of boxes I and II in (b1), respectively. (c1-c3) Air-heated specimen with shear deformation, σ_a=418 MPa and $N_f = 4.0 \times 10^4$ cycles, (c2) and (c3) are enlarged views of boxes I and II in (c1), respectively.

voids. Moreover, identification of deformation twins in α grains in Fig. 13(b2) and 13(c2) is conducted via HKL CHANNEL5 software according to the grain boundary of the twin mode for hexagonal close-packed (HCP) crystal structure in literature [46–48], and a tolerance of ± 5° deviation is used. Tensile twins at 85° and $<\bar{1}2\bar{1}0>$ are found in the nearby α grains of the two voids (Fig. 13(b2)) and the α grains near the crack propagation route (Fig. 13(c2)). This indicates that the twinning occurs in some α grains for the TC17 alloy during the LCF loadings at 400 ℃.

A minor fatigue crack ahead of the crack propagation route is also found in an α grain in Fig. 13(c1), and it shows narrow and transgranular features. The orientation of this α grain is shown as inset in Fig. 13(c1), and the SF on basal plane is 0.47. It shows that the direction of this fatigue crack in the plane view is parallel to the basal plane of this grain, which indicates that the formation of this fatigue crack is due to the basal slip. The results in Fig. 13 indicate that the mixed failure mode is a synergistic effect of ductile crack and fatigue crack. The internal voids and cracks similar to those in Fig. 13 were also observed in the section view for the initial specimen tested at 400 ℃ in vacuum-like environment. Therefore, the void and crack features should be common for the specimens failed from the mixed failure mode.

5. Conclusion

This paper studied the high-temperature fatigue behavior of TC17 titanium alloy and the influence of surface oxidation. Fatigue tests at room temperature and 400 ℃ were conducted for specimens in three conditions, i.e., initial specimens, vacuum-heated specimens and air-heated specimens. The influence of oxidation and the failure mechanism were analyzed in detail. The main conclusions are summarized as follows.

- The oxidation at 400 ℃ for 2 h made the specimen surface form an oxygen-rich layer, which had a thickness of hundreds of nanometers and improved the surface hardness.
- The fatigue crack initiation of the TC17 specimens at 400 ℃ in air and those with oxidation at room temperature in air was summarized as follows. Under high stress amplitudes, the oxidation promotes the surface crack initiation, and results in a negative effect on the fatigue life. With a decrease of stress amplitude, both surface and internal crack initiation could happen in HCF regime, and the negative effect of oxidation on the fatigue life decreased. At relatively lower stress amplitudes, the specimens mainly failed from internal crack initiation due to microstructure inhomogeneity and damage

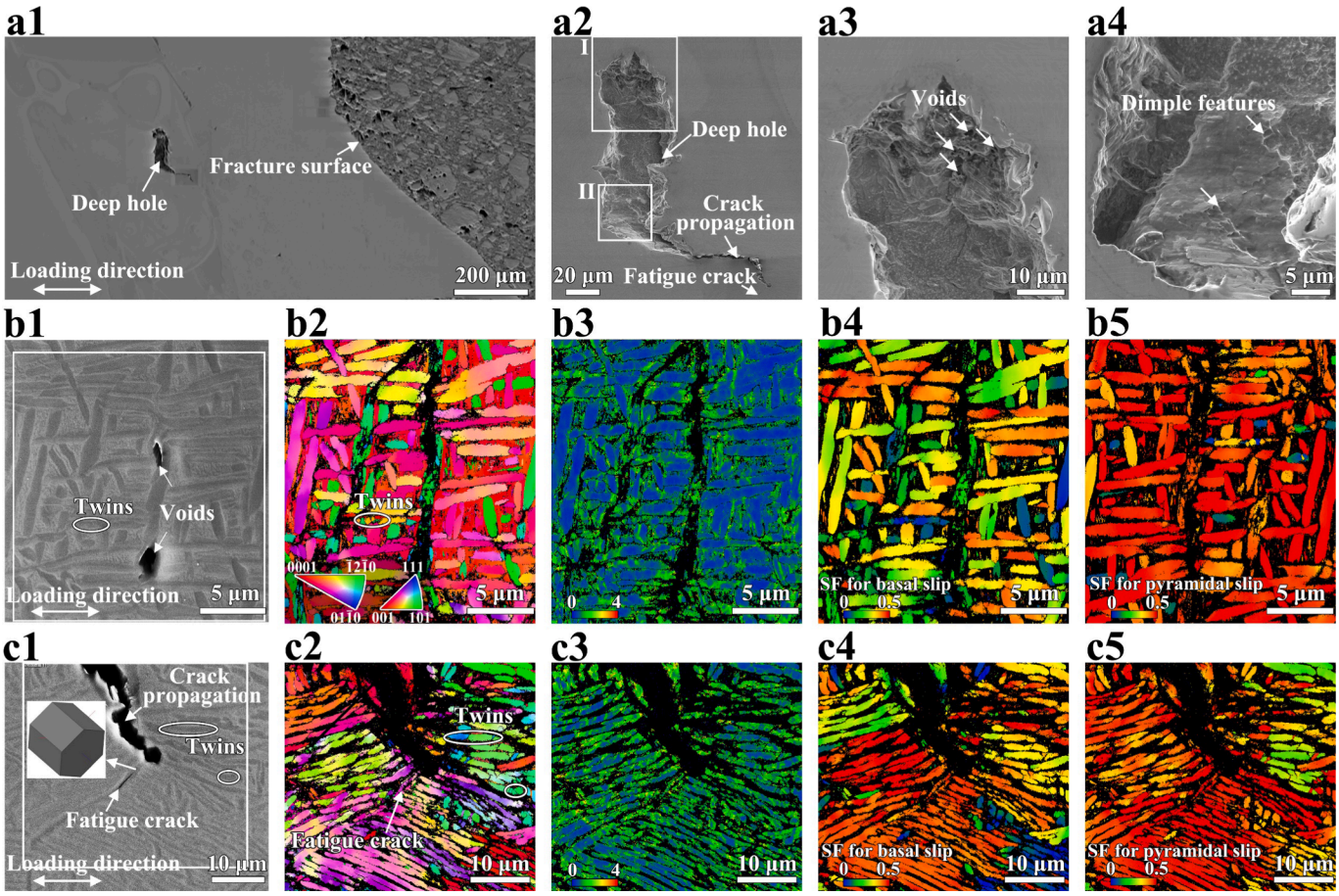

Fig. 13. Internal cracks and voids of an air-heated specimen tested at 400 ℃ in vacuum-like environment, σ_a=428 MPa and $N_f = 4.9 \times 10^4$ cycles. (a1) A section view of the specimen. (a2) An enlarged view of the deep hole in (a1). (a3) and (a4) are enlarged views of boxes I and II in (a2), respectively. (b1-b5) SEM image, IPF, KAM, SF on basal plane and pyramidal plane of the region including the two voids, respectively. Inset in (b2) is color legend. (c1-c5) SEM image, IPF, KAM, SF on basal plane and pyramidal plane of the region including the crack propagation in (a2), respectively. Inset in (c1) is the orientation of the α grain with fatigue crack.

accumulation. The crack initiation is irrespective of the influence of surface oxide in this situation.

- The specimens tested under high stress amplitudes at 400 ℃ and $R = 0.05$ in vacuum-like environment presented a mixed failure mode combining ductile cracks and fatigue cracks. The formation of ductile cracks should be attributed to the accumulation of local plastic strain and creep-like deformation. The failure of these specimens is a synergetic effect of ductile cracks and fatigue cracks. The surface oxidation in this state could restrict the development of ductile cracks around the surface, and it tends to improve the fatigue life for this failure mode.

CRediT authorship contribution statement

Gen Li: Methodology, Formal analysis, Investigation, Writing – original draft, Writing – review & editing. **Yiyun Guo:** Investigation, Writing – review & editing. **Shao-Shi Rui:** Investigation, Writing – review & editing. **Chengqi Sun:** Conceptualization, Methodology, Formal analysis, Investigation, Writing – original draft, Writing – review & editing, Funding acquisition, Supervision.

Declaration of Competing Interest

The authors declare that they have no known competing financial interests or personal relationships that could have appeared to influence the work reported in this paper.

Data availability

Data will be made available on request.

Acknowledgement

The authors gratefully acknowledge the support of the National Natural Science Foundation of China Basic Science Center for “Multi-scale Problems in Nonlinear Mechanics” (11988102), the National Natural Science Foundation of China (91860112) and International Postdoctoral Exchange Fellowship Program.

References

[1] Cervellon A, Cormier J, Mauget F, Hervier Z, Nadot Y. Very high cycle fatigue of Ni-based single-crystal superalloys at high temperature. Metall Mater Trans A 2018;49(9):3938–50.
[2] Cervellon A, Hemery S, Kurnsteiner P, Gault B, Kontis P, Cormier J. Crack initiation mechanisms during very high cycle fatigue of Ni-based single crystal superalloys at high temperature. Acta Mater 2020;188:131–44.
[3] Maier H. High-temperature fatigue of titanium alloys. Mater High Temp 1998;15 (1):3–14.
[4] Liu F, Chen Y, He C, Li L, Wang C, Li H, et al. Tensile and very high cycle fatigue behaviors of a compressor blade titanium alloy at room and high temperatures. Mater Sci Eng A 2021;811:141049.
[5] Li G, Sun C. High-temperature failure mechanism and defect sensitivity of TC17 titanium alloy in high cycle fatigue. J Mater Sci Technol 2022;122:128–40.
[6] Rugg D, Dixon M, Burrows J. High-temperature application of titanium alloys in gas turbines. Material life cycle opportunities and threats–an industrial perspective. Mater High Temp 2016;33(4–5):536–41.

[7] Satko D, Shaffer J, Tiley J, Semiatin S, Pilchak A, Kalidindi S, et al. Effect of microstructure on oxygen rich layer evolution and its impact on fatigue life during high-temperature application of α/β titanium. Acta Mater 2016;107:377–89.
[8] Gallo P, Berto F, F., Lazzarin, P.,. High temperature fatigue tests of notched specimens made of titanium Grade 2. Theor Appl Fract Mech 2015;76:27–34.
[9] Qian G, Jian Z, Pan X, Berto F. In-situ investigation on fatigue behaviors of Ti-6Al-4V manufactured by selective laser melting. Int J Fatigue 2020;133:105424.
[10] Zhao Z, Li Q, Zhang F, Xu W, Chen B. Transition from internal to surface crack initiation of a single-crystal superalloy in the very-high-cycle fatigue regime at 1100 °C. Int J Fatigue 2021;150:106343.
[11] Prakash D, Walsh M, Maclachlan D, Korsunsky A. Crack growth micro-mechanisms in the IN718 alloy under the combined influence of fatigue, creep and oxidation. Int J Fatigue 2009;31(11–12):1966–77.
[12] Mendez J, Mailly S, Villechaise P. Temperature and environmental effects on low cycle fatigue resistance of titanium alloys. Eur Struct Integrity Soc, 2002; Elsevier. p. 95-102.
[13] Foerch R, Madsen A, Ghonem H. Environmental interactions in high-temperature fatigue crack growth of Ti-1100. Metall Mater Trans A 1993;24(6):1321–32.
[14] Hardt S, Maier H, Christ H. High-temperature fatigue damage mechanisms in near-α titanium alloy IMI 834. Int J Fatigue 1999;21(8):779–89.
[15] Liu F, Peng H, Liu Y, Wang C, Wang Q, Chen Y. Crack initiation mechanism of titanium alloy in very high cycle fatigue regime at 400 ℃ considering stress ratio effect. Int J Fatigue 2022:107012.
[16] Stinville J, Martin E, Karadge M, Ismonov S, Soare M, Hanlon T, et al. Fatigue deformation in a polycrystalline nickel base superalloy at intermediate and high temperature: Competing failure modes. Acta Mater 2018;152:16–33.
[17] Zhao Z, Zhou R, Wang Z, Cai J, Chen B. High temperature fatigue behavior of a near-alpha titanium alloy. Int J Fatigue 2022;161:106918.
[18] Chen Y, Zhang H, Pan S, Song Y, Liu X, Liu W. Effects of service environment and pre-deformation on the fatigue behaviour of 2524 aluminium alloy. Arch Civil Mech Eng 2020;20:1–16.
[19] Ismarrubie Z, Yussof H, Sugano M. Fatigue damage mechanism of titanium in vacuum and in air. Procedia Eng 2012;41:1559–65.
[20] Heckel T, Christ H. Isothermal and thermomechanical fatigue of titanium alloys. Procedia Eng 2010;2(1):845–54.
[21] Maier H, Fischer F, Christ H. Environmental effects on the isothermal and thermomechanical fatigue behavior of a near-γ titanium aluminide. 2003: ASTM International.
[22] Cruchley S, Li H, Evans H, Bowen P, Child D, Hardy M. The role of oxidation damage in fatigue crack initiation of an advanced Ni-based superalloy. Int J Fatigue 2015;81:265–74.
[23] Li G, Ke L, Ren X, Sun C. High cycle and very high cycle fatigue of TC17 titanium alloy: stress ratio effect and fatigue strength modeling. Int J Fatigue 2022:107299.
[24] Sun C, Li Y, Xu K, Xu B. Effects of intermittent loading time and stress ratio on dwell fatigue behavior of titanium alloy Ti-6Al-4V ELI used in deep-sea submersibles. J Mater Sci Technol 2021;77:223–36.
[25] Saldaña L, Barrance V, Gonzalez-Carrasco J, Rodriguez M, Munuera L, Vilaboa N. Thermal oxidation enhances early interactions between human osteoblasts and alumina blasted Ti6Al4V alloy. J Biomed Mater Res A 2007;81(2):334–46.
[26] Mizuno Y, King F, Yamauchi Y, Homma T, Tanaka A, Takakuwa Y, et al. Temperature dependence of oxide decomposition on titanium surfaces in ultrahigh vacuum. J Vac Sci Technol A 2002;20(5):1716–21.
[27] Biswas A, Majumdar J. Surface characterization and mechanical property evaluation of thermally oxidized Ti-6Al-4V. Mater Charact 2009;60(6):513–8.
[28] Zhang Y, Zhang A, Li H. Surface oxidation and its effect on the fatigue property of TC4 alloy. Titan Ind Prog 2010;27(1):25–7.
[29] Gemelli E, Camargo N. Oxidation kinetics of commercially pure titanium. Revista Matéria 2007;12(3):525–31.
[30] Hass G. Preparation, structure, and applications of thin films of silicon monoxide and titanium dioxide. J Am Ceram Soc 1950;33(12):353–60.
[31] Hass G. Preparation, properties and optical applications of thin films of titanium dioxide. Vacuum 1952;2(4):331–45.
[32] Eshawish N, Malinov S, Sha W, Walls P. Microstructure and mechanical properties of Ti-6Al-4V manufactured by selective laser melting after stress relieving, hot isostatic pressing treatment, and post-heat treatment. J Mater Eng Perform 2021;30:5290–6.
[33] Gangwar K, Ramulu M. Friction stir welding of titanium alloys: a review. Mater Des 2018;141:230–55.
[34] Keist J, Palmer T. Development of strength-hardness relationships in additively manufactured titanium alloys. Mater Sci Eng A 2017;693:214–24.
[35] Sridhar B, Devananda G, Ramadancha K, Bhat R. Effect of machining parameters and heat treatment on the residual stress distribution in titanium alloy IMI-834. J Mater Process Technol 2003;139(1–3):628–34.
[36] Ebrahimi A, Zarei F, Khosroshahi R. Effect of thermal oxidation process on fatigue behavior of Ti-4Al-2V alloy. Surf Coat Technol 2008;203(3–4):199–203.
[37] Zhu W, Deng Y, Zhang Z, Tan G, Guo X. Effect of tensile stress response for oxide films on the fatigue failure behavior of anodized AA6082 alloys. Mater Sci Eng A 2022;850:143552.
[38] Dai W, Hao J, Li C, He D, Jia D, Zhang Y, et al. Residual stress relaxation and duty cycle on high cycle fatigue life of micro-arc oxidation coated AA7075-T6 alloy. Int J Fatigue 2020;130:105283.
[39] Altenberger I, Nalla R, Sano Y, Wagner L, Ritchie R. On the effect of deep-rolling and laser-peening on the stress-controlled low-and high-cycle fatigue behavior of Ti–6Al–4V at elevated temperatures up to 550 °C. Int J Fatigue 2012;44:292–302.
[40] Biallas G, Essert M, Maier H. Influence of environment on fatigue mechanisms in high-temperature titanium alloy IMI834. Int J Fatigue 2005;27(10–12):1485–93.
[41] Tokaji K. High cycle fatigue behaviour of Ti–6Al–4V alloy at elevated temperatures. Scr Mater 2006;54(12):2143–8.
[42] Liu F, Chen Y, He C, Liu Y, Wang C, Wang Q, et al. Creep-fatigue voids and sub-grain boundaries assisted crack initiation for titanium alloy in VHCF regime with high mean stress at 400 °C. Mater Sci Eng A 2022;844:143171.
[43] Gerland M, Lefranc P, Doquet V, Sarrazin-Baudoux C. Deformation and damage mechanisms in an α/β 6242 Ti alloy in fatigue, dwell-fatigue and creep at room temperature. Influence of internal hydrogen. Mater Sci Eng A 2009;507(1–2):132–43.
[44] Lefranc P, Doquet V, Gerland M, Sarrazin-Baudoux C. Nucleation of cracks from shear-induced cavities in an α/β titanium alloy in fatigue, room-temperature creep and dwell-fatigue. Acta Mater 2008;56(16):4450–7.
[45] Rodriguez P, Rao BS, K.,. Nucleation and growth of cracks and cavities under creep-fatigue interaction. Prog Mater Sci 1993;37(5):403–80.
[46] Sun C, Wu H, Chi W, Wang W, Zhang G. Nanograin formation and cracking mechanism in Ti alloys under very high cycle fatigue loading. Int J Fatigue 2023;167:107331.
[47] Crawforth, P., Towards a micromechanistic understanding of imparted subsurface deformation during machining of titanium alloys. 2014, University of Sheffield.
[48] Guan D, Mark Rainforth W, Ma L, Wynne B, Gao J. Twin recrystallization mechanisms and exceptional contribution to texture evolution during annealing in a magnesium alloy. Acta Mater 2017;126:132–44.